

## LASER PHOTO-CARRIER RADIOMETRY: TECHNIQUE AND APPLICATIONS TO SEMICONDUCTOR FABRICATION PROCESS NDE

Andreas Mandelis

Center for Advanced Diffusion-Wave Technologies, Department of Mechanical and Industrial Engineering, University of Toronto, Toronto CANADA

**Abstract:** Laser-induced infrared photo-carrier radiometry (PCR) is an emerging semiconductor NDT technology. PCR completely obliterates the thermal infrared emission band (8-12  $\mu\text{m}$ ), unlike the known photothermal signal types, which invariably contain combinations of carrier-wave and thermal-wave infrared emissions due to the concurrent lattice absorption of the incident beam and nonradiative heating. The PCR theory is briefly presented as infrared depth integrals of carrier-wave (CW) density profiles. Experimental aspects of this new methodology are given, including the determination of photo-carrier transport parameters (surface recombination velocities, carrier diffusion coefficients, recombination lifetimes and carrier mobilities) through modulation frequency scans. CW scanning imaging is also introduced. High-frequency, deep-defect PCR images thus obtained prove that very-near-surface (where optoelectronic device fabrication takes place) photo-carrier generation can be detrimentally affected not only by local electronic defects as is commonly assumed, but also by defects in remote wafer regions much deeper than the extent of the electronically active thin surface layer.

**Introduction:** In recent years the development of laser-induced infrared photothermal radiometry (PTR) of semiconductors in our laboratory as a quantitative methodology for the measurement of transport properties of semiconductors has led to several advances in the non-contact measurement of four transport parameters: bulk recombination lifetime, front and back surface recombination velocities and carrier diffusion coefficient in Si and GaAs. Reviews of the subject matter have been presented by Mandelis (1998) and Christofides et al. (2000). The major advantage of PTR over other photothermal techniques, such as photomodulated thermorefectance

(PMOR), has been found to be the higher sensitivity of PTR to the photo-excited free carrier-density-wave (the modulated-laser driven oscillating electronic diffusion wave (Mandelis (2001)) than PMOR (Wagner and Mandelis (1996); Salnick et al. (1997a)). This advantage exists due to domination of the free-carrier wave over the superposed thermal-wave (TW) contributions to the PTR signal. Even so, the ever-present thermal-wave contributions due to direct lattice absorption, followed by non-radiative energy conversion and blackbody (thermal infrared) emissions, have resulted in PTR signal interpretational and computational difficulties due to the large number of variables involved (Rodriguez et al. (2000)). Therefore, confidence in the measured values of the four electronic transport properties is always accompanied by the hurdle of having to assure uniqueness of the measured set of parameters in any given situation. Given the fundamental and practical importance of developing an all-optical, non-destructive and non-intrusive diagnostic methodology for monitoring the transport properties of semiconductors, and in view of the inability of photothermal semiconductor diagnostic methods (Christofides et al. (2000); Rosencwaig (1987)) to eliminate the thermal-wave contributions, we concluded that the search for a purely carrier-wave laser-based detection technique must move in the direction of isolating and filtering out the superposition of thermal-wave contributions to the infrared emission spectrum.

In a photo-excited semiconductor of bandgap energy  $E_G$ , an externally incident optical source such as a laser beam with super-bandgap energy photons  $\Sigma \omega_{vis} > E_G$  will be absorbed and can

generate free carriers which may subsequently follow several deexcitation pathways. Ultrafast decay to the respective bandedge (e.g. conduction band) through nonradiative transitions and emission of phonons, will raise the temperature of the semiconductor locally. The free carriers will further diffuse within their statistical lifetime and will recombine with carriers of the opposite sign across the bandgap or into impurity and/or defect states within the bandgap. The electron-hole recombination mechanism with or without phonon assistance will lead either to nonradiative energy conversion through phonon emissions (e.g. in indirect-gap semiconductors such as Si) which will further raise the temperature, or to radiative decay which will produce photons of near- or sub-bandgap energy. In actual semiconductor materials, there may be a distribution of impurity and defect states into which de-excitation may occur. Therefore, it is more relevant to consider the full spectral range of IR emissions from a photo-excited semiconductor crystal:  $\Sigma\omega_{IR} = \Sigma\omega(\lambda_D)$ . If the exciting super-bandgap radiation is intensity-modulated at frequency  $f = \omega/2\pi$ , then the photo-generated free carrier density constitutes a spatially damped carrier-density wave (CW) (or carrier-diffusion wave (Mandelis (2001))), which oscillates diffusively away from the generating source under its concentration gradient and recombines with a phase lag dependency on a delay time equal to its statistical lifetime,  $\tau$ , a structure- and process- sensitive property (van Roosbroeck and Shockley (1954)).

Under conditions that apply to a number of semiconductors (Mandelis et al. (2003)), electronic transitions in these materials occur essentially adiabatically, with minimum thermal energy exchange interactions across well-defined electronic state densities, leading to validation of Kirchhoff's Law of Detailed Balance (Kirchhoff (1898)) through complete thermal decoupling of the CW oscillator ensemble. A by-product of adiabaticity is that the IR spectra of thermal and carrier recombination emissions are independent of each other, a feature which is central to the realization of Photo-Carrier Radiometry (PCR).

### Principles of Photo-Carrier Radiometry

Figure 1 shows an elementary slice of thickness  $dz$  centered at depth  $z$  in a semiconductor slab. The crystal is supported by a backing, but is not necessarily in contact with the backing. A modulated laser beam at angular frequency  $\omega = 2\pi f$  and wavelength  $\lambda_{vis}$  impinges on the front surface of the semiconductor. The super-bandgap radiation is absorbed within a (short) distance from the surface, typically, a few  $\mu\text{m}$ , given by  $[\alpha(\lambda_{vis})]^{-1}$  where  $\alpha(\lambda_{vis})$  is the visible-range absorption coefficient of the pump radiation. The ensuing de-excitation processes generally involve radiative and nonradiative energy release components, resulting in the generation of an IR photon field in the semiconductor involving a relatively broad spectral bandwidth. At thermal and electronic equilibrium, assuming a one-dimensional geometry as a result of a large laser beam spotsize and/or thin sample, the emitted IR photons have equal probability of being directed toward the front or the back surface of the material. A detailed account of all IR emission, absorption, and reflection processes (Mandelis et al. (2003)) yields the expression for the total IR emissive power at the fundamental frequency across the front surface of the material in the presence of a backing support which acts both as reflector of semiconductor-generated IR radiation with spectrum centered at  $\lambda$ , and as emitter of backing-generated IR radiation centered at wavelength  $\lambda_b$

$$\begin{aligned}
 P_T \approx & \int_{\lambda_2}^{\lambda_1} d\lambda [1 - R_1(\lambda)] \left\{ \left( 1 + R_b(\lambda) [1 + R_1(\lambda)] \right) \varepsilon_o(\lambda) \right. \\
 & \int_0^L \Delta W_p(z, \omega; \lambda) dz + \left[ \left( 1 + R_b(\lambda) [1 + R_1(\lambda)] \right) W_o(T_o; \lambda) \right. \\
 & \left. \left. - W_p(T_b, \lambda) e(T_b, \lambda) [1 - R_1(\lambda)] \right] \int_0^L \varepsilon_{fc}(z, \omega, \lambda) dz \right\} \\
 & (1)
 \end{aligned}$$

where  $R_I$  is the front surface reflectivity,  $R_b$  is the backing support material reflectivity,  $\varepsilon_o(\lambda)$  is the background IR emission coefficient of the material,  $\varepsilon_{fc}(z, \omega; \lambda)$  is the IR emission coefficient due to the free photoexcited carrier wave,  $e(T_b, \lambda)$  is the spectral emissivity of the backing material,  $\Delta W_P(z, \omega, \lambda) dz$  is the harmonic IR emissive power due to the harmonically varying temperature of the sample,  $W_o(T_o; \lambda)$  is the unmodulated emissive spectral power per unit wavelength due to both Planck-mediated [ $W_{Po}(T_o, \lambda)$ ] and direct radiative [ $\eta_R W_{eR}(\lambda)$ ] emissions,  $W_P(T_b, \lambda)$  is the spectral emissive power per unit wavelength of the backing surface at temperature  $T_b$ , and  $[\lambda_1, \lambda_2]$  is the spectral bandwidth of the detector.  $W_{eR}(\lambda)$  is the spectral power per unit wavelength, the product of the recombination transition rate from band to band, or from bandedge to defect or impurity state, as the case may be, multiplied by the energy difference between initial and final states.  $\eta_R$  is the quantum yield for IR radiative emission upon carrier recombination into one of these states. During our experimental attempts to separate out carrier-wave and thermal-wave contributions which are always

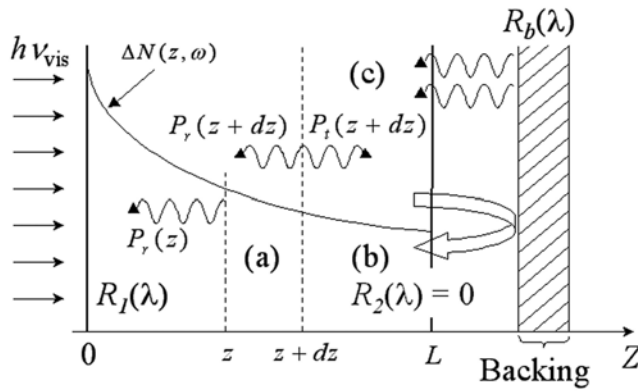


**Figure 1.** Cross-sectional view of contributions to front-surface radiative emissions of IR photons from a) a semiconductor strip of thickness  $dz$  at depth  $z$ ; b) re-entrant photons from the back surface due to reflection from a backing support material; c) emissive IR photons from the backing at thermodynamic temperature  $T_b$ . The carrier-wave depth profile  $\Delta N(z, \omega)$  results in a depth dependent IR absorption/emission coefficient due to free-carrier absorption of the infrared photon fields, both ac and dc.

strongly mixed as in Eq. (1), we found that they can be separated out effectively only through spectral filtering and bandwidth matching at the IR detector, thus introducing the PCR technique. Instrumental filtering of all thermal infrared emission contributions and bandwidth matching to the IR photodetector allows for all Planck-mediated terms to be eliminated from Eq. (1) yielding

$$P(\omega) \approx \int_{\lambda_2}^{\lambda_1} d\lambda [1 - R_1(\lambda)] \left[ (1 + R_b(\lambda)) \eta_R W_{eR}(\lambda) \int_0^L \varepsilon_{fc}(z, \omega; \lambda) dz \right] \quad (2)$$

The absorption coefficient (and, equivalently, assuming Kirchhoff's Law is valid, the emission coefficient) depends on the free-carrier density as (Smith (1978)

$$\varepsilon_{fc}(z, \omega; \lambda) = \alpha_{IRfc}(z, \omega; \lambda) = \frac{q\lambda^2}{4\pi^2 \varepsilon_{oD} c^3 n m^{*2} \mu} \Delta N(z, \omega; \lambda) \quad (3)$$

for relatively low CW densities. Here  $q$  is the elementary charge,  $\varepsilon_{oD}$  is the dielectric constant,  $c$  is the speed of light in the medium,  $n$  is the refractive index,  $m^*$  is the effective mass of the carrier (electron or hole) and  $\mu$  is the mobility. This allows the PCR signal to be simply expressed in the form

$$P(\omega) \approx F(\lambda_1, \lambda_2) \int_0^L \Delta N(z, \omega) dz \quad (4)$$

with

$$F(\lambda_1, \lambda_2) = \int_{\lambda_2}^{\lambda_1} [1 - R_1(\lambda)] \left( [1 + R_b(\lambda)] [1 + R_1(\lambda)] \right) \eta_R W_{eR}(\lambda) C(\lambda) d\lambda \quad (5)$$

The PCR signal is the integration of Eq. (4) over the image of the detector on the sample and thus is directly proportional to the depth integral of the carrier density in the sample. Consequently, the relative lateral concentration of any defects that affect the carrier density, either by enhancing recombination or altering diffusion coefficients, can be determined by scanning the surface of the wafer with the PCR probe. In addition, frequency scan techniques can be used with the appropriate carrier diffusion model to obtain quantitative values for the four transport parameters (Rodriguez et al. (2000)). This quantitative technique can be combined with surface scans to provide quantitative imaging of the semiconductor sample.

## PCR Imaging NDT of Electronic Defects in Si Wafers

### *Instrumentation and Signal Characteristics*

The experimental implementation of laser infrared photo-carrier radiometry is similar to the typical PTR set-up for semiconductors (Mandelis (1998); Rodriguez et al. (2000)), with the crucial difference being that the spectral window of the IR detector and optical filter, and the modulation frequency response of the preamplifier stage, must be tailored through spectral bandwidth matching to a combination of carrier recombination emissions and effective spectral filtering of the Planck-mediated thermal infrared emission band. Conventional PTR utilizes photoconductive liquid-nitrogen-cooled HgCdTe (MCT) detectors with spectral bandwidth in the 2-12  $\mu\text{m}$  range. This includes the thermal infrared range, 7-12  $\mu\text{m}$ , and only part of the electronic emission spectrum at shorter wavelengths. From experiments with several IR detectors and bandpass optical filters we concluded that emissive infrared radiation from electronic CW recombination in Si is centered mainly in the spectral region below 3  $\mu\text{m}$ . The IR detector was a switchable-gain InGaAs element (ThorLabs model PDA400), 1-mm in diameter, with spectral response in the 800 – 1750 nm range, peak response at 1550 nm and frequency bandwidth from dc to 10 MHz. The preamplifier was incorporated into the detector housing, a design which delivered optimal signal-to-noise ratio expressed as a NEP figure of  $2.9 - 8.2 \times 10^{-12} \text{ W}/\sqrt{\text{Hz}}$ . The detector was outfitted with a specialty long-pass optical filter from Spectrogon featuring very steep cut-on (5% at 1010 nm, 78% at 1060 nm, and transmission range 1042 – 2198 nm). The cut-on quality of the filter is crucial in PCR as it must block any pump radiation leakage from reaching the highly sensitive detector. Short-wavelength filtering of optical density 5 or 6 is usually required. The samples were placed on an aluminum backing which acted as a support, heater, and signal amplifier by redirecting the forward emitted IR photons back toward the detector (Mandelis *et al.* (2003)), Fig.1. The incident Ar-ion laser beam size was 1.06 mm and the power was 20-24 mW. The detector was proven extremely effective in cutting off all thermal infrared radiation: Preliminary measurements using non-electronic materials (metals, thin foils and rubber) showed no responses whatsoever.

### *PCR Imaging of Deep Sub-Surface Electronic Defects*

Figure 2 shows line scans with the excitation laser beam scanning the front (polished) surface of a 20  $\Omega\text{cm}$  p-type Si wafer and the IR detector on the same side. Based on the backing

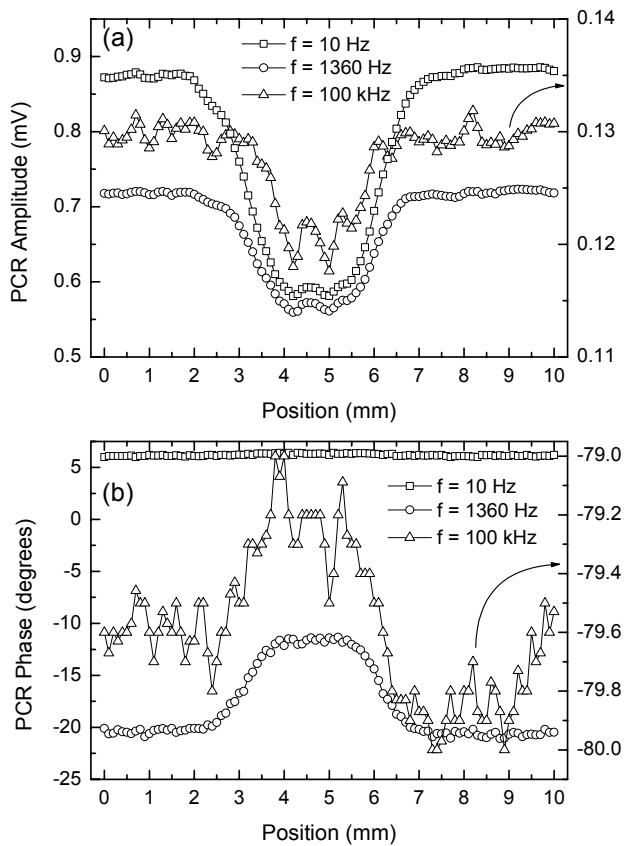
results, for maximum signal strength the sample was resting on a mirror. At all three selected modulation frequencies, the PCR amplitude decreases when the laser beam scans over the defect region, consistent with the expected CW density decrease as the back-surface defect efficiently traps carriers and removes them from further diffusion and potential radiative recombination. The PCR phase scan remains essentially constant at 10 Hz, Fig. 2b, as the diffusion-wave centroid is solely determined by the ac carrier-wave diffusion length (van Roosbroeck and Shockley (1954); Mandelis et al. (2003))

$$L_{ac}(\omega) = \sqrt{\frac{D^* \tau}{1 + i \omega \tau}} \quad (6)$$

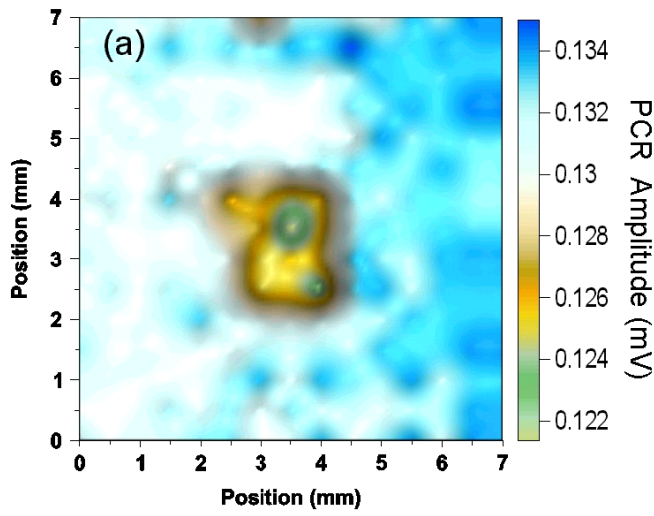
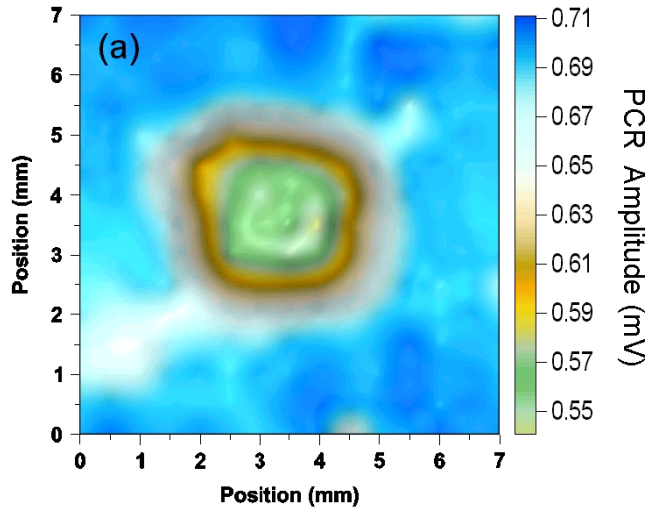
where  $\tau$  is the lifetime and  $D^*$  is the ambipolar carrier diffusion coefficient. This particular wafer was measured to have  $\tau \cong 1$  ms and  $D^* \cong 12$  cm<sup>2</sup>/s, which yields an  $|L_{ac}(10 \text{ Hz})| \cong 1.1$  mm. Therefore, the CW centroid lies well beyond the thickness of the wafer ( $\sim 630$   $\mu\text{m}$ ) and no phase shift can be observed. At the intermediate frequency of 1360 Hz,  $|L_{ac}| \cong 373$   $\mu\text{m}$ , well within the bulk of the wafer. In this case, a phase lead appears within the defective region. This occurs because the CW spatial distribution across the body of the wafer in the defective region is weighed more heavily toward the front surface on account of the heavy depletion occurring at, and near, the back surface. As a result, the CW centroid is shifted toward the front surface, manifested by a phase lead. Finally, at 100 kHz,  $|L_{ac}| \cong 44$   $\mu\text{m}$ . Nevertheless, Fig. 2a shows that there is still PCR amplitude contrast at that frequency, accompanied by a small phase lead, Fig. 2b. Figure 3 shows images of the back-surface defect obtained through front-surface inspection at the optimum contrast frequency of 1360 Hz. Figure 4 shows the same scan at 100 kHz. At this frequency the PCR image clearly shows the highest spatial resolution of the back-surface defect possible. The PCR phase, Fig. 4b, shows details of the central defect as well as the

**Figure 2.** Line scans over an p-Si wafer region with back-surface mechanical damage. (a) PCR amplitude; (b) PCR phase. The wafer is resting on a mirror support. Laser power: 24 mW.

radially diverging defect structures at the base of the central defect, like a "zoomed in" version of the 1360 Hz image, Fig. 3b. Both PCR images clearly reveal internal sub-structure of the central defect, which was invisible at 1360 Hz. In a manner reminiscent of conventional propagating wavefields, image resolution increases with decreasing carrier wavelength,  $|L_{ac}|$ . Under front-surface inspection and precise depth profilometric control by virtue of the PCR modulation-frequency-adjustable carrier-wave diffusion length, Eq. (6), Figs. 3 and 4 show for the first time that with today's high-quality, long-lifetime industrial Si wafers, one can observe full images of sharp carrier-wave density contrast due to underlying defects very deep



inside the bulk of a Si wafer. Specifically, high frequency PCR imaging reveals so far unknown very long-range effects of carrier interactions with deep sub-surface defect structures and the detrimental ability of such structures to decrease the overall free photoexcited-carrier density far away from the defect sites at or near the front surface where device fabrication takes place. This phenomenon may be important toward device fabrication improvement through careful selection of substrate wafers with regard to deep bulk growth and manufacturing defects which were heretofore not associated with device performance. Further PCR imaging experiments with shorter lifetime Si wafers have shown that it may be beneficial to use lower quality starting substrates in order to avoid the full effects of deep sub-surface defects on the electronic quality of the upper (device-level) surface.



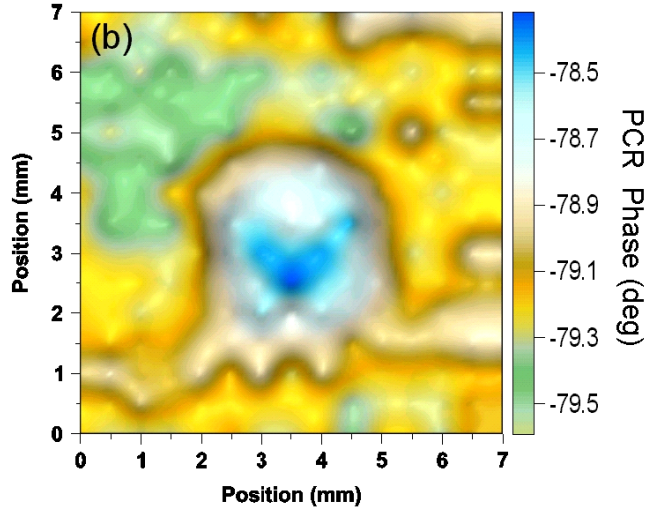
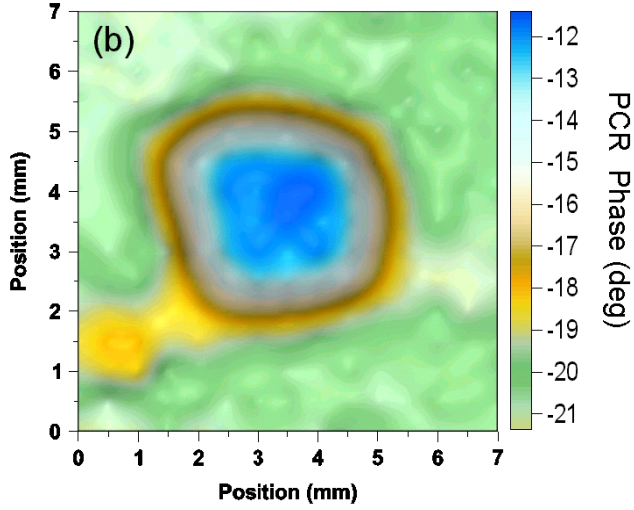


**Figure 3.** Scanning imaging of back-surface defect in the p-Si wafer using front-surface inspection. Laser beam radius: 518  $\mu\text{m}$ . Frequency: 1360 Hz. (a) PCR amplitude; (b) PCR phase.

**Figure 4.** Scanning imaging of back-surface defect in the p-Si wafer using front-surface inspection. Laser beam radius: 518  $\mu\text{m}$ . Frequency: 100 kHz. (a) PCR amplitude; (b) PCR phase.

deep sub-surface defects which may result in unpredictably variable performance and electronic quality of the upper (device-level) surface.

### Quantitative PCR Measurements Of Electronic Transport Properties

The PCR image contrast of Figs. 3 and 4 can, in principle, be quantified by use of the CW term in Eq. (4), appropriately modified to accommodate the defective region:

$$\Delta P(\omega) \approx F_2(\lambda_1, \lambda_2) \left[ \int_0^L \Delta N(z, \omega) dz - \int_0^L \Delta N_d(z, \omega) dz \right] \quad (7)$$

where  $\Delta P(\omega)$  is the difference in signal between the intact and defective regions. This is a complex quantity, so it can be separated out into amplitude and phase components. The apparent

simplicity of this expression is due to the fact that the sub-surface defects considered here are on the back surface of the wafer and their presence mostly impacts the value of the back-surface recombination velocity  $S_2$  (Mandelis (2001)), while the bulk transport parameters and the terms comprising the prefactor  $F(\lambda_1, \lambda_2)$ , remain essentially unaltered for a thin damage layer in an otherwise homogeneous semiconductor. If these conditions are not fulfilled, then a more complete expression of the carrier recombination related emissions must be used to quantify PCR contrast due to distributed sub-surface electronic defect structures.

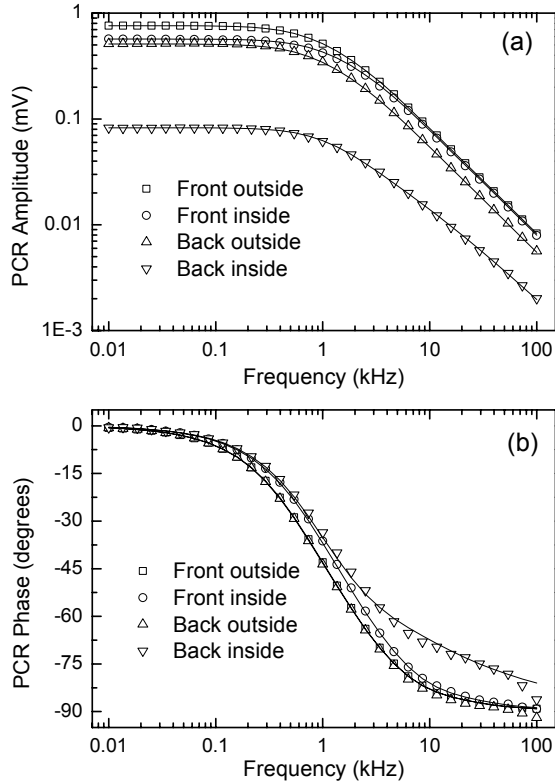


**Figure 5:** Front- and back-surface PCR frequency scans inside and outside a defect area of a p-Si wafer on aluminum backing. Best fits to the data of Eq. (4) were made using the carrier-density-wave field  $\Delta N(z, \omega)$  expression Eq. (9.106) in Mandelis (2001).

Detector: InGaAs; beam size: 1.4 mm; Ar-ion laser power: 20 mW. (a)

Amplitudes and (b) phases. Best fit parameters:

Front intact region:  $\tau = 1$  ms;  $D^* = 12$  cm<sup>2</sup>/s,  $S_1 = 10$  cm/s,  $S_2 = 210$  cm/s.

Front inside the defect:  $\tau = 1$  ms;  $D^* = 14.9$  cm<sup>2</sup>/s,  $S_1 = 25$  cm/s,  $S_2 = 300$  cm/s.

Back intact region:  $\tau = 1$  ms;  $D^* = 12$  cm<sup>2</sup>/s,  $S_1 = 10$  cm/s,  $S_2 = 200$  cm/s.

Back inside the defect:  $\tau = 1$  ms;  $D^* = 5$  cm<sup>2</sup>/s,  $S_1 = 450$  cm/s,  $S_2 = 130$  cm/s.

The mild mechanical defect on the back surface of the p-type Si wafer that generated the images of Figs. 3 and 4 proved to be too severe for our sensitive InGaAs photodetector: upon scanning the affected surface the PCR signal vanished within the region of the defect, apparently due to the highly efficient trapping of the photogenerated free carriers by the high density of near-surface electronic defect states. Therefore, a different region of the same wafer was chosen to create a visually undetectable defect by simply touching the back surface of the wafer with paper. Then PCR frequency scans were performed on both sides of the material, outside and inside the defect region, Fig. 5. The inherent instrumental transfer function was removed by introducing an indirect normalization method based on the fact that in the high frequency regime both HgCdTe and InGaAs detectors monitor the same electronic processes (Mandelis et al. (2003)). All curves shown here were normalized by the same transfer function obtained by this method. The PCR theoretical model involved carrier-wave IR emissions using diffusion-wave field expressions (Mandelis (2001), Chap. 9.12), with adjustable electronic transport coefficients (Rodriguez et al. (2000); Ikari et al. (1999)). The effect of the back-surface defect was modeled as a change in the recombination velocity  $S_2$  (front-surface probing) only. When the wafer was turned over, the

definitions of  $S_1$  and  $S_2$  were reversed. Regarding the  $D^*$  values, those outside the defect remained constant for both sides of the wafer, however, the  $D^*$  value from the back inside the defect region was relatively low. The high sensitivity of the InGaAs detector to the electronic state of the inspected surface is probably responsible for this discrepancy, as the theoretical phase fit is poor at high frequencies ( $> 1$  kHz) within that region, an indication of near-surface depth inhomogeneity of transport properties.

## Conclusions

Laser infrared photo-carrier radiometry (PCR) has been introduced. This technique is a photonic method based on carrier diffusion-wave diagnostics. Based on the theoretical foundations and the first few experimental case studies using industrial-quality Si wafers, there are excellent prospects for PCR as an *in-situ* quality control NDT technology in semiconductor processing. Its local monitoring nature surpasses the currently available techniques for non-destructive, non-contact monitoring and imaging of deep electronic defects in Si wafers, for measuring free-carrier transport properties without the need for auxiliary electric circuit fabrication and electrode application. PCR can become a valuable NDT technology as it can monitor local values of carrier mobilities and other transport properties at several intermediate stages of device fabrication. A noteworthy feature of high frequency PCR imaging is that it has revealed for the first time a very long-range effect of carrier interactions with deep sub-surface defect structures and the detrimental ability of such structures to decrease the overall free photoexcited-carrier density in locations far away from the defect sites at or near the front surface where device fabrication takes place. Therefore, PCR may become an important tool toward device fabrication improvement through careful selection of substrate wafers with regard to deep bulk growth and manufacturing defects which were heretofore not associated with device performance.

## Acknowledgments

I wish to acknowledge the support of the Natural Sciences and Engineering Research Council of Canada (NSERC) for a Discovery Grant, and of Materials and Manufacturing Ontario (MMO) for a Collaborative Contract which made this research possible.

## References

- Christofides, C., Nestoros, M. & Othonos, A. 2000. in *Semiconductors and Electronic Materials*. Progress Photoacoustic and Photothermal Phenomena Vol. IV (A. Mandelis and P. Hess, eds., SPIE, Bellingham, WA, 2000), Chap. 4.
- Ikari, T., Salnick, A. & Mandelis, A. 1999. *Journal of Applied Physics*. 85: 7392.
- Kirchhoff, G. 1898. *Abhandlungen über Emission und Absorption*. (M. Planck, Ed., Verlag von Wilhelm Engelmann, Leipzig), 11-36.
- Mandelis, A. 1998. *Solid-State Electron*. 42(1).
- Mandelis, A. 2001. *Diffusion-Wave Fields: Mathematical Methods and Green Functions*, Springer-Verlag, NY, Chap. 9.
- Mandelis, A., Batista, J. & Shaughnessy, D. 2003. *Phys. Rev. B* 67: 205208.
- Rodriguez, M.E., Mandelis, A., Pan, G., Nicolaidis, L., Garcia, J.A. & Riopel, Y. 2000. *J. Electrochem. Soc.* 147: 687.
- Rosencwaig, A. 1987. in *Photoacoustic and Thermal-Wave Phenomena in Semiconductors*. (A. Mandelis, Ed., North-Holland, New York), Chap. 5.
- Salnick, A., Jean, C. & Mandelis, A. 1997a. *Solid-State Electron*. 41: 591.

Smith, R.A. 1978. *Semiconductors, 2nd Ed.* (Cambridge Univ. Press, Cambridge), 118.

van Roosbroeck, W. & Shockley, W. 1954. *Phys. Rev.* 94: 1558.

Wagner, R.E. & Mandelis, A. 1996. *Semicond. Sci. Technol.* 11: 300.